



Thermodynamic modeling of the Al-Co-Cr-Fe-Ni high entropy alloys supported by key experiments



Marlena Ostrowska^{a,*}, Paola Riani^a, Brandon Bocklund^b, Zi-Kui Liu^b, Gabriele Cacciamani^a

^a Department of Chemistry and Industrial Chemistry, University of Genoa, Italy

^b Department of Materials Science and Engineering, The Pennsylvania State University, University Park, PA 16802, USA

ARTICLE INFO

Article history:

Received 1 September 2021

Received in revised form 27 October 2021

Accepted 8 November 2021

Available online 19 November 2021

Keywords:

CALPHAD Thermodynamic modeling High Entropy Alloys (HEA) Al-Co-Cr Fe-Ni ESPEI

ABSTRACT

Al-Co-Cr-Fe-Ni alloys have been modeled by computational thermodynamics according to the CALPHAD approach using literature data and results of a few key experiments performed in this work. As a result, an Al-Co-Cr-Fe-Ni thermodynamic database has been developed, based on the thermodynamic assessments of all the binary and ternary subsystems and the addition of a few quaternary interaction parameters. The assessment was supported by ESPEI (Extensible Self-optimizing Phase Equilibria Infrastructure), a tool for thermodynamic database development within the CALPHAD method. Computed phase equilibria in the quinary system are in good agreement with experimental data from the literature and the present experiments.

© 2021 Elsevier B.V. All rights reserved.

1. Introduction

High Entropy Alloys (HEA) have been intensively studied in recent years with the hope to find among them new materials showing improved properties with respect to the classical alloys [1]. HEAs based on 3d transition metals and in particular Co, Cr, Fe and Ni, have been especially investigated as a possible replacement of classical superalloys for high temperature applications [2–6] and [7]. Another element to be taken into account is Al, already included in classical superalloys for many reasons, such as formation of the gamma prime phase in the alloy bulk, the thermal grown oxide (TGO) on the alloy surface, and stabilization of bcc phase, as well as reduction of density.

The present work focused on phase equilibria in the Al-Co-Cr-Fe-Ni system through the CALPHAD approach [8] supported by a few key experiments. It is known that the CALPHAD method enables the prediction of phase equilibria in complex multicomponent materials, such as HEAs, as a function of composition and other state variables, once thermodynamic functions of the phases in lower order systems are defined. These calculations can support experimental investigations and provide fundamental information, essential to accelerate the development of new materials.

Despite the Al-Co-Cr-Fe-Ni system is the most frequently investigated HEA, the experimental information on the influence of alloying elements (especially Co, Cr and Fe) on the quinary phase equilibria is still very limited and validation of such system purely based on the literature data would be insufficient. Therefore, in the present work, effects of the alloying elements on phase equilibria were examined in annealed samples. The obtained information on phase formation and phase compositions was used for the improvement of the database developed in the present work.

2. Thermodynamic modeling using CALPHAD method

A CALPHAD thermodynamic database contains a set of thermodynamic functions describing Gibbs energies of individual phases in a given system. The Gibbs energy is expressed according to the Compound Energy Formalism (CEF) [9], a general approach which allows to select the most appropriate model for each phase in the framework of the same formalism. According to CEF, the different constituents of a phase (neutral atoms, ions, vacancies, etc.) are distributed in one or more sublattices, where they mix according to the classical solution theory (adopting ideal, regular, subregular, etc., behavior) with different interaction parameters in different sublattices.

The detailed description of how the total Gibbs energy is evaluated for individual phases can be found in our previous publication [10] and in more detail in the recent overview by Liu [11].

* Correspondence to: Dipartimento di Chimica e Chimica Industriale Università di Genova via Dodecaneso, 31 I-16146 Genova, Italy.

E-mail address: ostrowska.marlena@gmail.com (M. Ostrowska).

2.1. Thermodynamic modeling of binary and ternary sub-systems

The Al-Co-Cr-Fe-Ni system contains 10 binary and 10 ternary sub-systems: modeling of all of them is needed to build the multi-component database. In general, the parameters adopted from published assessments were included in the new database, provided that they are compatible with our phase models. In some cases, however, more or less extended reassessment was needed in order to be consistent with the models adopted in our database. In systems where a reassessment was performed, parameters were optimized using the ESPEI (Extensible Self-optimizing Phase Equilibria Infrastructure) software package [12]. ESPEI is a tool for thermodynamic database development within the CALPHAD method. It optimizes CALPHAD model parameters and quantifies the uncertainty of the model parameters using Markov Chain Monte Carlo (MCMC). ESPEI supports adjustment of parameters simultaneously in multi-component systems and related sub-systems, using PyCalphad as the computing engine [13].

The CEF model of a specific phase is usually related to its crystallographic structure with sublattices corresponding to its Wyckoff positions. However, the number of sublattices should be kept as low as possible, without losing the ability to correctly reproduce the experimentally observed phase equilibria. This can be achieved by merging in a single sublattice the crystallographic sites having similar coordination and being occupied by atoms similar in size. Using a lower number of sublattices reduces the number of parameters that have to be evaluated during modeling.

For disordered solid solutions such as liquid, fcc, bcc, hcp, one sublattice is typically needed, because the unique crystallographic site can be occupied by all elements. In the case of the solid solutions fcc, bcc and hcp, an additional sublattice containing vacancies (Va) is added to represent the interstitial sites.

For stoichiometric intermetallic phases, each sublattice contains only a single element. If the crystal structure is unknown, the model is determined by the experimentally observed composition. For nonstoichiometric intermetallic phases with a solubility range, more than one element is placed in the same sublattice.

For ordered phases derived from disordered solid solutions a common description is possible. For simplicity, a 2-sublattice model was chosen for the ordered bcc phase (B2). Both sublattices are equivalent. In addition to all the present elements, they also contain vacancies (Va) in order to reproduce the relatively high concentration of thermal vacancies detected in B2 (e.g. Al-Co and Al-Ni [14]). A 4-sublattice model would be necessary to describe other ordered bcc structures, such as D0₃ and B32, but they are seldom observed in HEA systems, and it would also require the introduction of many interaction parameters. The L1₂ phase (ordered fcc structure) is also described with two sublattices, which cannot describe other type of fcc ordering, such as L1₀. Such structures, however, are not common in the systems considered in the present work.

All the solid phases present in the mentioned binary and ternary sub-systems are listed in Table 1 together with the thermodynamic models used in the present database.

2.1.1. Binary systems

Parameters describing all 10 binary sub-systems present in the Al-Co-Cr-Fe-Ni have been added to the multicomponent database.

Re-assessment of the Al-Co system [10] is based on parameters assessed by Stein et al. [15] with modifications regarding vacancies in A2 and B2 and re-assessment of the bundle of phases close to the 4:13 stoichiometry, which were experimentally investigated by Priputen et al. [16]. These are four phases having monoclinic or orthorhombic structure with composition ranging from Al₇₁Co₂₉ to Al₇₇Co₂₃.

The binary parameters describing the Co-Cr system were adopted from Wang et al. [17]. The original parameters of the σ phase were slightly modified to compensate the different choice of the lattice stabilities of the σ phase. For the Co-Fe system, the description by Wang et al. [18] was used together with parameters concerning magnetic ordering assessed by Ohnuma et al. [19].

The remaining binary sub-systems, Al-Cr [20], Al-Fe [21], Al-Ni [20], Co-Ni [22], Cr-Fe [23], Cr-Ni [24] and Fe-Ni [25], were adopted from the available assessments without modifications.

2.1.2. Ternary systems

All 10 ternary subsystems of the Al-Co-Cr-Fe-Ni have been assessed. Parameters for most of them were taken from the literature and many of them required modifications. The main incompatibilities were related to thermodynamic models used to describe topologically close-packed (TCP) phases, such as μ and σ , as well as to the binary parameters used to describe sub-systems, especially in case of less recent assessments. The detailed description of model selection for μ and σ phases and application of these models in modeling of a series of selected ternary systems can be found in our previous work [26].

The most recent assessment of Al-Co-Cr system by Liu et al. [27] is incompatible with our database due to differences in binary parameters and models describing the σ phase. Therefore, the system was completely reassessed in this work based on the experimental data from Liu et al., Moskvitina et al., and Ishikawa et al. [27–29]. The Al-Co-Fe system was assessed in our previous work [10]. The stabilities of intermetallic phases rich in Al, namely Co₂Al₉ and FeAl₂, were recently revised, after the publication of new experimental data by Zhu et al. [30]. The parameters describing the Al-Co-Ni system were taken from the assessment by Wang and Cacciamani [14], however, the A1, A2 and B2 parameters were re-optimized using ESPEI [12]. The parameters from Wang and Cacciamani were the starting values for the optimization. A slight improvement of equilibria between the fcc and bcc phases was obtained. The description of the Al-Cr-Fe system was based on the assessment by Wang et al. [31], however, due to differences in binary parameters, the assessment had to undergo considerable modifications in major phases, such as liquid, bcc, fcc, γ -LT and γ -HT. The parameters regarding the Al-Cr-Ni system assessed by Wang and Cacciamani [20] were adopted in the present work. The Al-Fe-Ni assessment by Zhang et al. [32] was implemented in the database. Due to the discrepancies in binary parameters the equilibria between fcc and bcc phases were revised and adjusted to the available experimental data.

The Co-Cr-Fe system was assessed in the present work using ESPEI [12] for the optimization process with the experimental data from Dombre et al. [33], who determined various isothermal sections at temperatures ranging from 800 to 1300 °C. The resulted isothermal sections compared with the experimental data were presented in our previous publication [26]. The parameters describing the Co-Cr-Ni system were adopted from Cacciamani et al. [34]. Due to differences in Co-Cr binary parameters, the A1, A2 and σ phases were remodeled. The Co-Fe-Ni system was assessed in the present work based on the available experimental information regarding the equilibria between A1 and A2 phases in the temperature range 500–800 °C determined by Koester and Haehl [35], as well as data regarding magnetic transition investigated by Kase [36]. The Cr-Fe-Ni thermodynamic database reported by Franke and Seifert [25] combined with bcc parameters from Miettinen [37] was used as a base for our assessment. However, in both publications, the model used to describe the σ phase is not compatible with ours, therefore the σ phase was reassessed in the present work.

Isothermal section of all 10 ternary subsystems calculated at 1100 °C with the present database are shown in Fig. 1.

Table 1
Solid phases, their structural information and models used in the present database.

| Phase | Structure information | Model |
|---|---|---|
| A2 | cI2 - W - Im $\bar{3}m$ | (Al,Co,Cr,Fe,Ni,Va) ₁ (Va) ₃ |
| B2 | cP2 - CsCl - Pm $\bar{3}m$ | (Al,Co,Cr,Fe,Ni,Va) _{0.5} (Al,Co,Cr,Fe,Ni,Va) _{0.5} (Va) ₃ |
| A1 | cF4 - Cu - Fm $\bar{3}m$ | (Al,Co,Cr,Fe,Ni) ₁ (Va) ₁ |
| L1 ₂ | cP4 - AuCu ₃ - Pm $\bar{3}m$ | (Al,Co,Cr,Fe,Ni) _{0.75} (Al,Co,Cr,Fe,Ni) _{0.25} (Va) ₁ |
| A3 | hP2 - Mg - P6 ₃ /mmc | (Al,Co,Cr,Fe,Ni) ₁ (Va) _{0.5} |
| μ | hR13 - W ₆ Fe ₇ - R-3 m - D8 ₅ | (Al,Co) ₄ (Al,Co,Cr,Fe,Ni) ₂ (Al,Co,Cr,Fe,Ni) ₁ (Al,Co,Cr,Fe,Ni) ₆ |
| σ | tP30 - CrFe - P4 ₂ /mnm - D8 ₆ | (Al,Co,Cr,Fe,Ni) ₂ (Al,Co,Cr,Fe,Ni) ₈ (Al,Co,Cr,Fe,Ni) ₅ |
| C14 | hP12 - MgZn ₂ - P6 ₃ /mmc | (Al,Co,Cr,Fe,Ni) ₁ (Al,Co,Cr,Fe,Ni) ₂ |
| C15 | cF24 - MgCu ₂ - Fd-3 m | (Al,Co,Cr,Fe,Ni) ₁ (Al,Co,Cr,Fe,Ni) ₂ |
| C36 | hP24 - MgNi ₂ - P6 ₃ /mmc | (Co,Cr,Ni) ₁ (Co,Cr,Ni) ₂ |
| FeAl ₂ | aP18 - Fe ₅ (Fe _{0.5} Al _{0.5}) ₃ Al ₁₀ - P1 | (Co,Cr,Fe,Ni) ₁ (Al) ₂ |
| MoPt ₂ | oI6 - MoPt ₂ - Immm | (Cr,Ni) ₁ (Cr,Ni) ₂ |
| MoSi ₂ | tI6 - MoSi ₂ - I4/mmm - C11 _b | (Al,Co,Cr,Ni) ₁ (Al,Co,Cr,Ni) ₂ |
| DO ₁₉ | hP8 - Mg ₃ Cd - P6 ₃ /mmc | (Al,Co,Cr,Ni) ₁ (Al,Co,Ni) ₃ (Va) ₂ |
| CoAl ₃ | mS36 - (Co _{0.88} Ni _{0.12}) ₄ Al _{12.1} | (Co,Ni) _{0.255} (Al) _{0.745} |
| NiAl ₃ | oP16 - Fe ₃ C | (Co,Fe,Ni) ₁ (Al) ₃ |
| CrAl ₄ | oS584 - Cr _{23.76} (Cr _{0.23} Al _{0.77}) ₂₁ Al _{96.10} | (Cr,Fe) ₁ (Al, Va) ₄ |
| CrAl ₅ | mP48 - CrAl ₅ - P2 | (Cr,Fe) ₁ (Al) ₅ |
| Ni ₂ Al ₃ | hP5 - Ni ₂ Al ₃ - | (Al) ₃ (Al,Co,Cr,Fe,Ni) ₂ (Co,Ni,Va) ₁ |
| Co ₂ Al ₅ | hP28 - Co ₂ Al ₅ | (Co,Fe,Ni) ₂ (Al) ₅ |
| Fe ₂ Al ₅ | oS24 - FeAl _{2.8} - Cmcmm | (Co,Cr,Fe,Ni) ₂ (Al) ₅ |
| Co ₂ Al ₉ | mP22 - Co ₂ Al ₉ | (Co,Fe,Ni) ₂ (Al) ₉ |
| Ni ₃ Al ₄ | cI112 - Ni ₃ Ga ₄ | (Co,Ni) ₃ (Al) ₄ |
| Cr ₄ Al ₁₁ | aP15 - Mn ₄ Al ₁₁ - P-1 | (Cr) ₄ (Al) ₁₁ |
| O-Co ₄ Al ₁₃ | oP102 - Co ₄ Al ₁₃ | (Co) _{0.24} (Al) _{0.76} |
| Y-Co ₄ Al ₁₃ | m* - C2/m | (Co,Ni) _{0.245} (Al) _{0.755} |
| M ₄ Al ₁₃ | mS102 - Fe ₄ Al ₁₃ - C2/m | (Co,Cr,Fe,Ni) _{0.235} (Al) _{0.6275} (Al, Va) ₁₃₇₅ |
| Ni ₅ Al ₃ | oS16 - Pt ₅ Ga ₃ | (Ni) ₅ (Al) ₃ |
| Cr ₇ Al ₄₅ | mC104 - V ₇ Al ₄₅ - C2/m | (Cr,Fe,Ni) ₇ (Al) ₄₅ |
| Fe ₅ Ni ₂₄ Al ₇₁ | | (Fe) _{0.5} (Ni) _{0.24} (Al) _{0.71} |
| EPSILON3 | oP - Cr ₂₀ Fe _{2.5} Al _{77.5} | (Cr) _{0.21} (Fe) _{0.02} (Al) _{0.77} |
| γ -HT | cI52 - Cu ₅ Zn ₈ - I4-3/m - D8 ₂ | (Al,Cr,Fe) ₂ (Al,Cr,Fe,Ni) ₃ (Cr,Fe,Ni) ₂ (Al,Fe) ₆ |
| γ -LT | | (Al,Cr) ₁₂ (Al,Cr,Fe,Ni) ₅ (Al,Cr,Fe,Ni) ₅ (Al,Cr,Fe) ₄ |
| DAICoNi | P10/mmm | (Al) ₁₄ (Al,Co,Ni) ₁ (Co,Ni) ₅ |
| XAlCoNi | mS26 - - C2/m | (Al) ₉ (Co) ₂ (Co,Ni) ₂ |
| Y ₂ AlCoNi | oI96 - - Immm | (Al) ₃ (Co,Ni) ₁ |
| Fe ₃ NiAl ₁₀ | mP22 - Co ₂ Al ₉ - P2 ₁ /a | (Fe,Ni) ₂ (Al) ₅ |
| FeNiAl ₉ | P10/mmm | (Fe,Ni) ₂ (Al) ₉ |
| O1 | oI366 - - Immm | (Al,Cr,Fe) ₂₈ (Al) ₇₂ |
| Cr ₁₆ Fe ₁₂ Al ₇₂ | | (Al,Cr,Fe) ₂₈ (Al) ₇₂ |
| Cr _{11.5} Fe ₆ Al _{82.5} | hR1389 - - R-3 | (Cr) _{0.9} (Al,Cr,Fe) ₂₂ (Al) ₁ |

3. Experimental validation of Al-Co-Cr-Fe-Ni alloys

While the influence of Al in the quinary system Al-Co-Cr-Fe-Ni has been extensively investigated by various authors [38–49], the information about the impact of other elements on the constitution and microstructure of these alloys is very limited. In the present work, equilibrated alloys with various amounts of Co, Cr and Fe have been prepared in order to provide the missing information on phase equilibria, that can be compared with our calculations and used for improvement of the database.

3.1. Materials and methods

Seven samples were prepared from a mixture of commercial purity elemental metals (>99.99%). Their nominal compositions are reported in Table 2. They were melted several times in a vacuum arc furnace under Ar atmosphere using Zr as a getter. Multiple melting improved homogeneity of the samples. Each sample was approximately 1 g and in all cases the weight loss after melting was less than

0.5 mass%. Samples were placed inside tantalum crucibles which were sealed in quartz tubes under Argon atmosphere and annealed for around 2160 h at 1050°C followed by air cooling.

The polished sections of alloys were prepared by standard metallographic procedures. Microstructure of the samples was examined, and the phase compositions were determined using Scanning Electron Microscope (Zeiss EVO 40, Carl Zeiss, Oberkochen, Germany) equipped with an Energy Dispersive X-ray spectroscope (EDX Pentafet, Oxford Instruments, Oxfordshire, U.K.). The BSE images were taken with magnification between 700 and 10000x. The acceleration voltage (EHT) was set to 20 kV and working distance (WD) to 8 mm.

The present phases were identified by X-Rays Diffraction (X'Pert MPD Philips, Almedo, Netherlands) from a surface of a bulk material. XRD patterns were recorded with a step scan mode ranging from 10 to 100° with the step size of 0.02° and 4 s time per step. The Match!3 software [50] was used for the qualitative analysis of the obtained XRD patterns. The quantitative analysis was done by Rietveld refinement method by means of FullProf program [51].

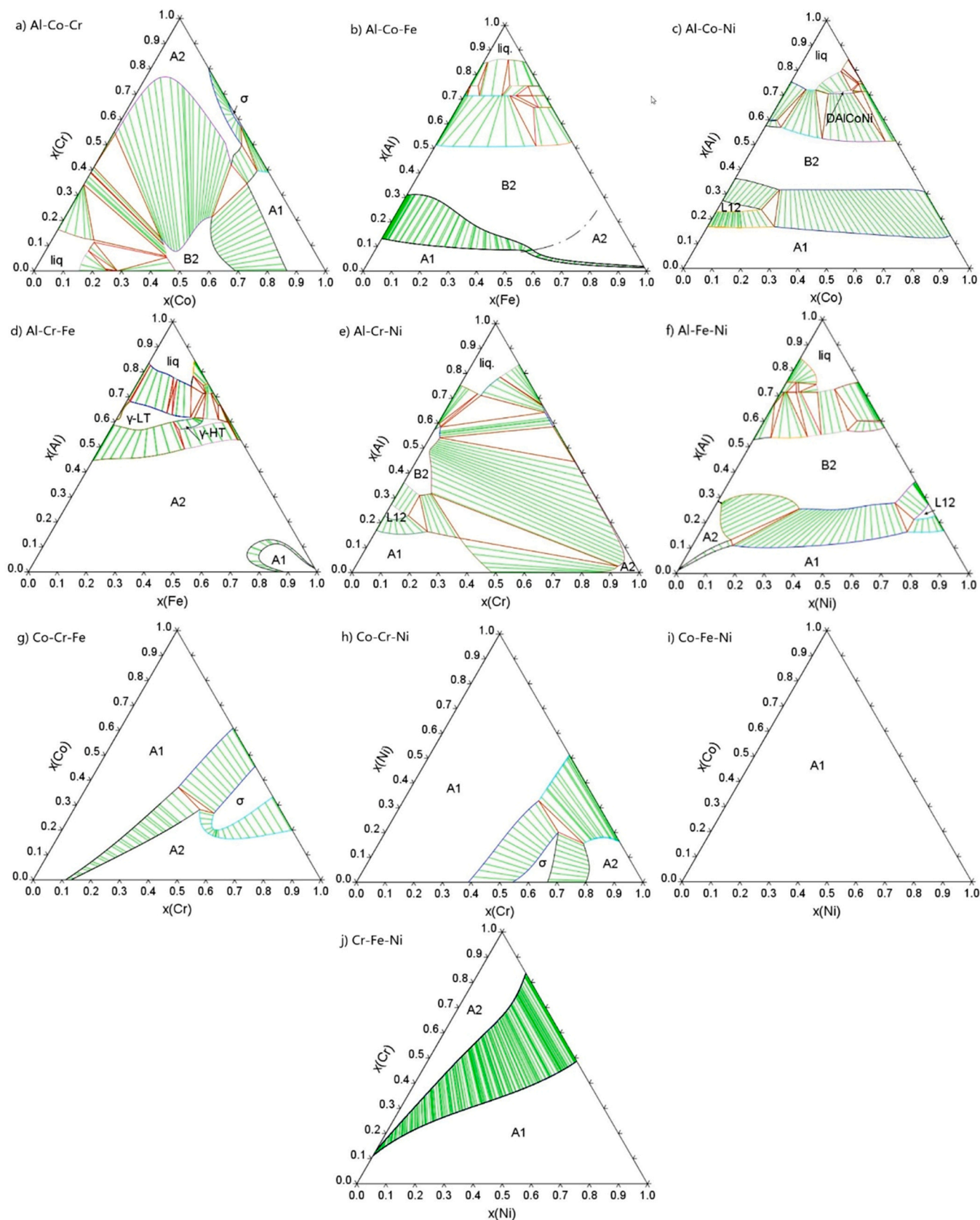


Fig. 1. Isothermal sections at 1100 °C calculated with the present database of a) Al-Co-Cr, b) Al-Co-Fe, c) Al-Co-Ni, d) Al-Cr-Fe, e) Al-Cr-Ni, f) Al-Fe-Ni, g) Co-Cr-Fe, h) Co-Cr-Ni, i) Co-Fe-Ni and j) Cr-Fe-Ni systems.

Table 2
Nominal composition of prepared samples.

| Name | Nominal composition |
|--------|----------------------------|
| ARef | AlCoCrFeNi |
| ACo0.5 | AlCo _{0.5} CrFeNi |
| ACo1.5 | AlCo _{1.5} CrFeNi |
| ACr0.5 | AlCoCr _{0.5} FeNi |
| ACr1.5 | AlCoCr _{1.5} FeNi |
| AFe0.5 | AlCoCrFe _{0.5} Ni |
| AFe1.5 | AlCoCrFe _{1.5} Ni |

3.2. Experimental results

Fig. 2 and Fig. 3 show representative SEM images of the annealed samples. Two or three types of phases were identified in the samples. The reference sample (Fig. 2) is three-phase: darker phase separated by a light phase and a mix of the lighter phase and a third gray phase inside the darker phase. This gray phase precipitated inside the lighter one can be seen also in Fig. 3d-f.

The XRD profiles with assigned phases are shown in Fig. 4. The compositions of individual phases in the SEM images were measured using EDX point analysis and are reported in Table 3. The matrix, darker in micrographs of Fig. 3, is rich in Al and Ni and assigned as the ordered B2 phase. The brighter regions correspond to the

disordered A1 phase rich in Co, Cr and Fe while the less bright areas are associated with the disordered bcc A2 phase rich in Cr.

In two samples (ACr1.5 and AFe0.5), the σ phase was observed, which should not be stable at annealing temperature of 1050 °C. According to the calculations, the A2 phase transforms into σ phase at 887 °C for the sample ACr1.5 and 969 °C for AFe0.5; moreover, the A2 and σ phases have very similar compositions. Taking all the information into account it was assumed that the σ phase precipitated during cooling of the samples.

4. Validation with the experimental data

For the verification of the database, the calculated equilibrium phases and their compositions were compared with the experimental information obtained in the present work and reported in the literature, which have been critically reviewed and carefully chosen for the validation process, considering their reliability and usability. Due to the sluggish diffusion in HEAs, it is expected that a long time is necessary to bring an alloy into the equilibrium state. However, some published results have been obtained after very short annealing times and it is questionable if the reported phase compositions correspond to an equilibrium state. This factor has been taken into account while selecting the data for the validation in this work. The collected data were used to improve the quality of

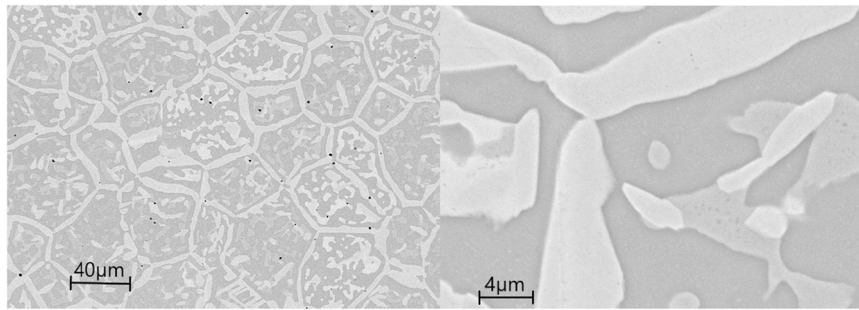


Fig. 2. SEM images of the ARef sample.

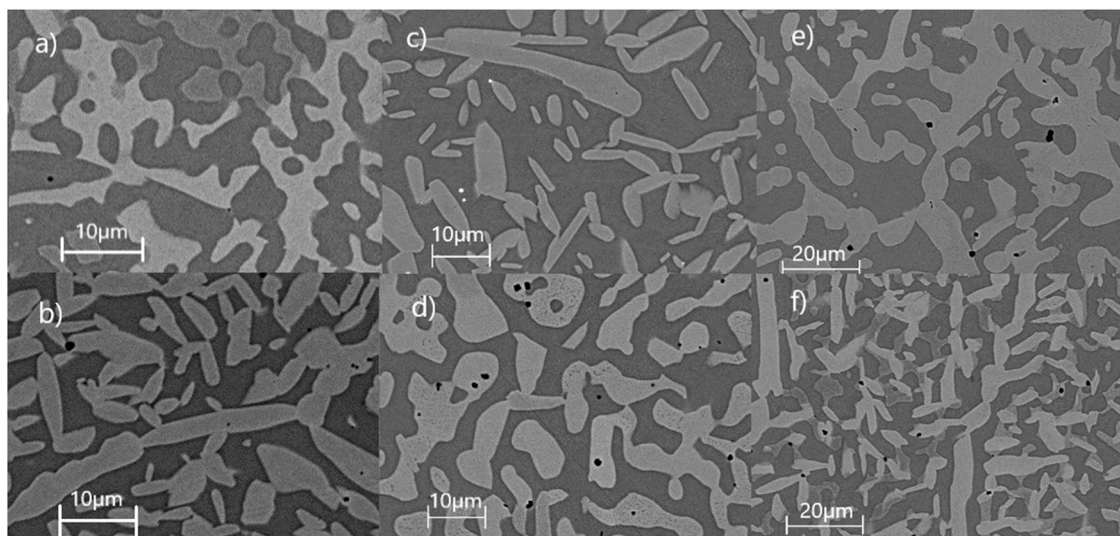


Fig. 3. SEM images of a) ACo0.5, b) ACo1.5, c) ACr0.5, d) ACr1.5, e) AFe0.5 and f) AFe1.5 samples.

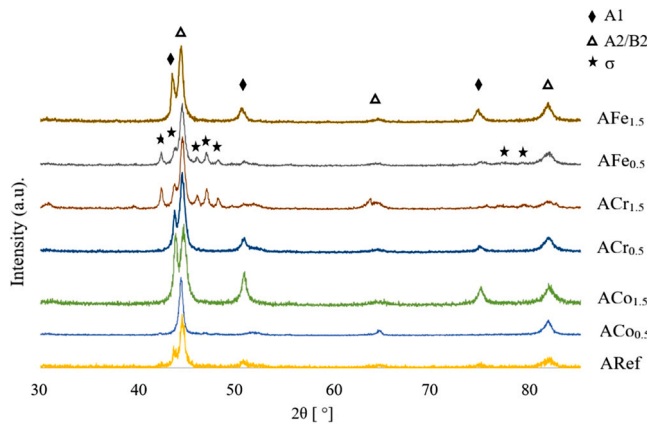


Fig. 4. XRD profiles of the samples annealed at 1050 °C for 2160 h.

calculations by adding or adjusting parameters for metastable end members in lower order systems.

4.1. Literature review of the Al-Co-Cr-Fe-Ni system

The Al-Co-Cr-Fe-Ni is the most frequently studied HEA. In 2009 Kao et al. [38] prepared a series of arc-melted samples with different Al contents, annealed at 1100°C for 24 h and water quenched. The authors investigated the microstructure of as-cast, annealed and deformed samples by means of SEM, EDS and XRD. The influence of Al was also studied by Chou et al. [39] in the same year. They prepared a series of Al_xCoCrFeNi samples with x ranging from 0 to 2. They were kept at 1100 °C for 24 h and water quenched; phases were identified by XRD. Shun and Du [49] investigated samples with the Al_{0.3}CoCrFeNi composition by means of SEM, EDS and TEM techniques. The specimens underwent annealing at 700 and 900 °C for 72 h and quenching in cold water. Wang et al. [43] examined the evolution of the structure of the Al_xCoCrFeNi samples (0 < x < 1.8) using high temperature XRD, SEM and TEM. The samples for microstructural measurements were annealed at 900 and 1100 °C for 2 h. Additionally, transition temperatures were determined by means of DTA. In 2015 Tang et al. [48] compared the microstructure and phase composition of as-cast samples and samples that underwent homogenizing treatment by applying hot isostatic pressure (HIP) and annealing at 1150°C for 50 h followed by cooling at 10°C/min. The same fabrication method (HIP) was applied by Zhang et al. [45] at 1250 °C for 50 h. Afterwards, the samples Al_{0.3}CoCrFeNi and Al_{0.7}CoCrFeNi were heat-treated at 700 and 1250 °C for 500 and 1000 h, respectively. The present phases were analysed by means of XRD, SEM, EBSD, and APT techniques. Subsequently, Butler and Weaver [47] investigated the high temperature phases and compared the results with the predicted ones using the Thermo-Calc database TCNI8 [52]. A series of samples were annealed at 700 °C for 1000 h and at 1050°C for 520 h, followed by water quenching.

Rao et al.[46] studied 3 alloys: Al_{0.3}CoCrFeNi, Al_{0.5}CoCrFeNi and Al_{0.7}CoCrFeNi by means of EBSD, TEM and APT. The samples were heated at 1250 °C for 50 h followed by furnace cooling. The obtained data were compared with thermodynamic calculations in the same work. Wang et al. [40] examined the microstructure of the alloys with equimolar composition aged at 600, 800, 1000 and 1200 °C for 168 h and water quenched. Sun et al. [53] prepared a set of samples with different Al to Co ratios. They were arc-melted, homogenized at 800°C and 1000°C for 30 days and quenched in cold water. Their phase constituents and microstructure were measured by SEM, EDS and XRD.

A series of alloys with different Cr content were investigated by Cieslak et al. [54]. They were prepared by two different synthesis methods: arc-melting and sintering from blended mixture of metallic powders. The first ones were then annealed at 1000°C for 72 h

Table 3 Phase compositions (at%) measured by EDX point analysis.

| Sample | Phases identified using XRD | A1 | | | A2 | | | B2 | | | σ | | |
|--------|-----------------------------|-----|------|------|-----|------|------|------|------|-----|------|-----|------|
| | | Al | Co | Fe | Al | Co | Fe | Al | Co | Fe | Al | Co | Fe |
| ARef | A1, A2, B2 | 5.6 | 23.8 | 29.2 | 2.0 | 16.6 | 49.2 | 32.3 | 18.9 | 7.2 | 12.5 | | |
| ACo0.5 | A2, B2 | | | | 2.4 | 10.2 | 47.4 | 34.9 | 11.8 | 5.7 | 12.7 | | |
| ACo1.5 | A1, B2 | 5.6 | 30.1 | 24.1 | | | | 31.5 | 23.5 | 8.4 | 11.3 | | |
| ACr0.5 | A1, B2 | 6.0 | 25.4 | 34.1 | | | | 30.5 | 20.8 | 5.4 | 15.4 | | |
| ACr1.5 | A1, B2, σ | 6.0 | 23.2 | 27.9 | | | | 32.3 | 17.9 | 8.4 | 12.0 | | |
| AFe0.5 | A1, B2, σ | 6.1 | 29.0 | 15.5 | | | | 33.4 | 19.6 | 8.0 | 7.7 | 2.4 | 18.5 |
| AFe1.5 | A1, A2, B2 | 5.6 | 20.1 | 37.3 | 3.5 | 13.5 | 43.4 | 31.9 | 17.8 | 6.9 | 15.3 | 2.7 | 23.6 |
| | | | | | | | | | | | | 2.4 | 50.4 |
| | | | | | | | | | | | | 2.7 | 52.7 |
| | | | | | | | | | | | | | 13.7 |
| | | | | | | | | | | | | | 22.9 |

Table 4
Annealing and cooling conditions of Al-Co-Cr-Fe-Ni samples reported in the literature.

| Author | Annealing conditions | Cooling conditions |
|------------------------|---------------------------------|--------------------|
| this work | 1050°C for 2160 h | in air |
| 2009_Kao[38] | 1100°C for 24 h | cold water |
| 2009_Chou[39] | 1100 °C for 24 h | cold water |
| 2009_Shun[49] | 700 and 900 °C for 72 h | cold water |
| 2014_Wang[43] | 900 and 1100 °C for 2 h | cold water |
| 2015_Tang[48] | 1150°C for 50 h | 10°C/min |
| 2016_Zhang[45] | 700 °C for 500 h | |
| | 1250 °C for 1000 h | |
| 2017_Butler[47] | 1050°C for 520 h | cold water |
| 2017_Rao[46] | 1250°C for 50 h | furnace cooling |
| 2017_Wang[40] | 800, 1000 and 1200 °C for 168 h | cold water |
| 2019_Sun[53] | 800°C for 720 h | cold water |
| | 1000°C for 720 h | |
| 2019_Cieslak[54] | 1000°C for 336 h | cold water |
| 2020_Stryzhyboroda[41] | 750 °C for 48 h | cold water |
| | 1000 °C for 24 h | |
| | 1300 °C for 6 h | |

while the samples prepared from as-compacted metallic powder were annealed at the same temperature for 2 weeks. All samples underwent quenching. In addition to structural studies, the transition temperatures were identified using the Differential Scanning

Calorimetry (DSC) technique. Stryzhyboroda et al. [41] investigated the transition temperatures of as-cast samples by means of DTA measurement with the heating rate of 20 K/min. Additionally, the microstructural analysis was carried out on annealed samples by means of SEM equipped with EDS and EBSD detectors. Samples with different Al content were annealed at 1300, 1000 and 750 °C for 6, 24 and 48 h, respectively. The summary of the annealing conditions by different authors is shown in Table 4.

4.2. Comparison and discussion

After the combination of the binary and ternary subsystems and extrapolation to the quinary Al-Co-Cr-Fe-Ni system and comparison with the experimental data it was observed that the stability of the A2 phase was too low with respect to the experimental information. As a consequence of the missing A2 phase, the mismatch between the calculated and measured composition of the B2 phase was quite high. Moreover, the calculated solidus and liquidus temperatures in the quinary system were slightly lower than the measured ones. The mismatch required the addition of a few metastable quaternary mixing parameters: $G(A2,Co,Cr,Fe,Ni:VA) = +482,300 - 100 * T$, $G(liquid,Al,Co,Cr,Fe:Va) = +120,000$ and $G(liquid,Al,Co,Cr,Ni:Va) = +120,000$. Additionally, in order to improve the fit in the A1 phase composition the ternary A1 parameters were revised, in particular in the Al-Cr-Fe system. The modifications

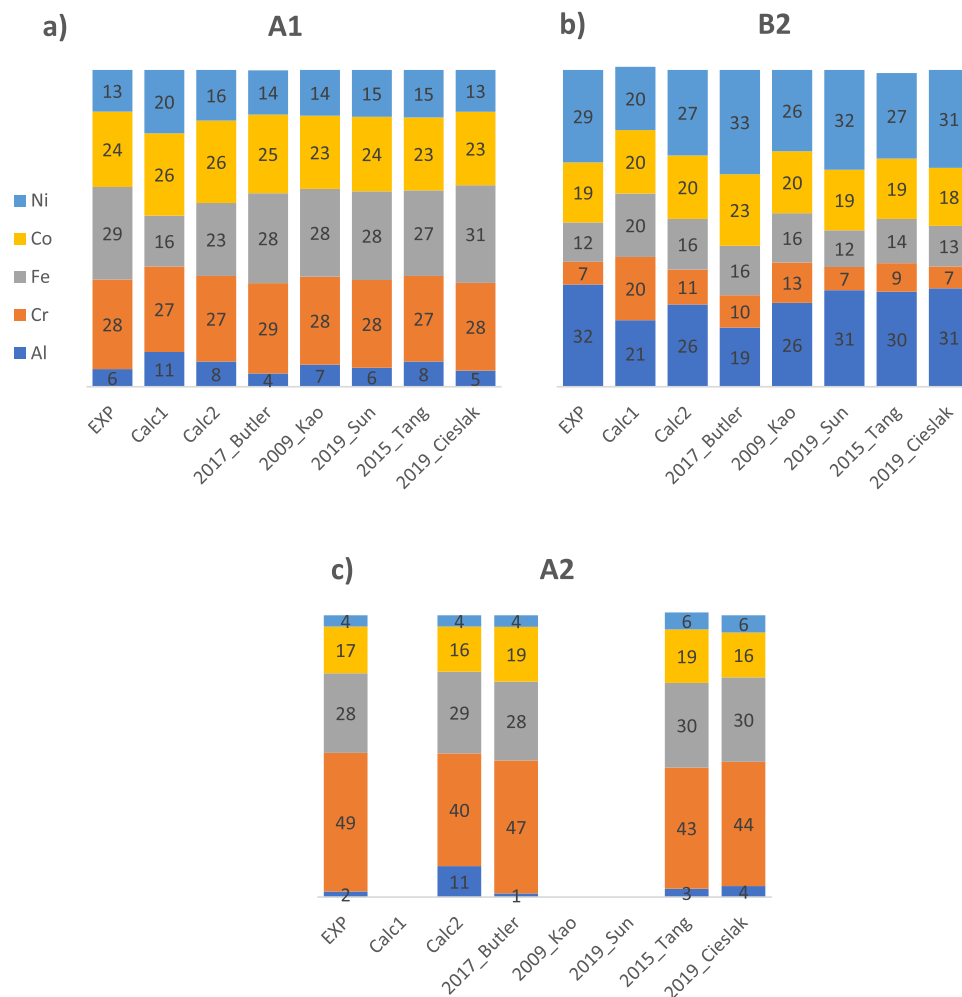


Fig. 5. Experimental phase compositions obtained in this work for the ARef sample annealed at 1050°C (EXP) compared with the calculated values before (Calc1) and after (Calc2) optimization and with various experimental results from the literature [38,47,48,53,54] for a) A1, b) B2 and c) A2 phases.

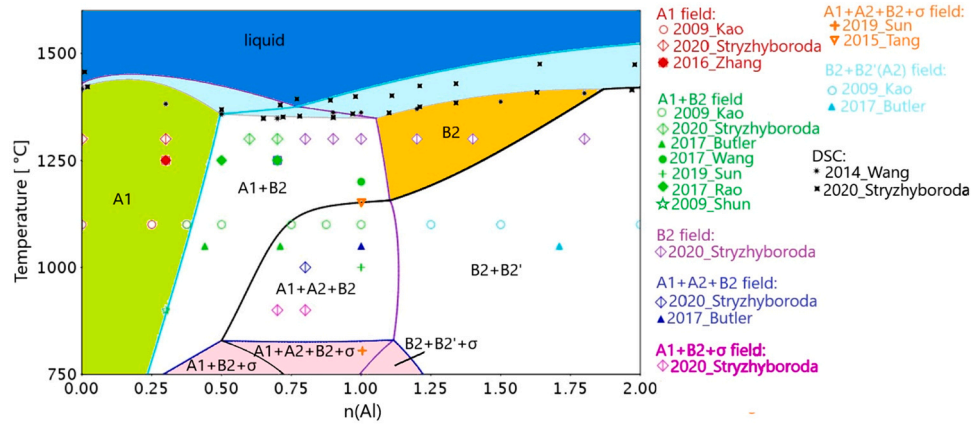


Fig. 6. Calculated vertical section of the $\text{Al}_x\text{CoCrFeNi}$ system compared to the experimental data regarding stable phases [38,40,41,45–49,53,54] and transformation temperatures [41,43].

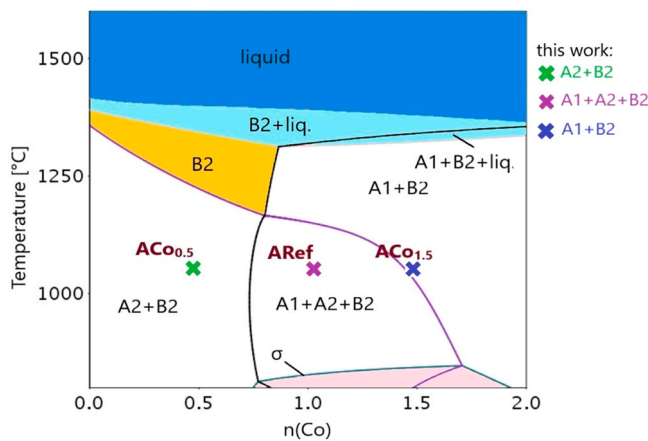


Fig. 7. Calculated $\text{AlCo}_x\text{CrFeNi}$ vertical section for $0 < x < 2$. The nominal compositions of the investigated samples are added to the figures. Blue – liquid single phase; yellow – B2 single phase; light blue – liquid is present; pink – σ is present.

significantly improved the agreement between calculations and experiments.

4.2.1. Equimolar composition

The average phase compositions measured in this work in the ARef sample with equimolar composition and the selected literature data for the equimolar AlCoCrFeNi alloy at the temperature ranging from 1000 to 1150 °C [38,47,48,53,54] are compared in Fig. 5 with the calculated values before (Calc1) and after (Calc2) the optimization in order to check reliability of the multicomponent database.

The overall agreement between the experimental and calculated data for the AlCoCrFeNi composition after the revision of the parameters is very good. The biggest discrepancy can be observed in the A2 phase, where the calculated amount of Al is higher than the measured one.

The discrepancies between various authors may result from the fact that the samples were annealed at slightly different temperatures, as reported in Table 4 (between 1000 and 1150 °C). Moreover, the annealing time varies significantly (from 24 h to 720 h). Finally, some sintered samples were quenched in cold water [38,47,54], whereas others were cooled at a controlled rate 10 °C/min [48] or in the air (this work). The A2 phase was not observed by some authors

[38,53]. It can result from the fact that it is very difficult to distinguish between ordered and disordered bcc phases using only the XRD measurements, due to the low intensity of the peaks differentiating the two phases, especially when the presence of the additional phase is not clear in the SEM images.

4.2.2. Effect of Al

The influence of Al is presented in the calculated $\text{Al}_x\text{CoCrFeNi}$ isopleth (Fig. 6) with $0 < x < 2$. The experimental data points are added. The data regarding stable phases were collected from several references [38,40,41,45–49,53,54], whereas the transformation temperatures were reported by Wang et al. [43] and Stryzhyboroda et al. [41].

Some reported experimental results are not in agreement with each other. It is especially the case of the A2 and B2 phases. As already mentioned, this might be caused by the fact that it is very difficult to correctly distinguish these phases using only the EDS and XRD measurements. Additionally, Tang et al. [48] observed the σ phase at 1150 °C for the equimolar composition. It is highly unlikely that the σ phase is stable at such a high temperature in this quinary system; it is also in contradiction with several other experimental data reported for this composition. The presence of the σ phase can be a result of the slow cooling at a controlled rate of 10 °C/min. During such slow cooling the phases that are stable at lower temperatures may precipitate. The σ phase was also observed in the $\text{Al}_{0.7}\text{CoCrFeNi}$ and $\text{Al}_{0.8}\text{CoCrFeNi}$ samples annealed at 900 °C by Stryzhyboroda et al. [41]. Additionally, the same authors reported that a single phase B2 is stable at 1300 °C for the compositions above 0.8 mol Al, while according to our calculations the A1 phase is stable up to around 1.05 mol Al at that temperature. The solidus and liquidus temperatures measured by Stryzhyboroda et al. [41] and solidus temperatures reported by Wang et al. [43] are reproduced in a satisfactory way by the calculations, with a maximum difference of 40 °C.

4.2.3. Effect of Co

The presence of all phases observed in the samples have been correctly predicted by the calculations as shown in Fig. 7. Nominal compositions of our samples are marked at the equilibration temperature in the figure which shows the calculated $\text{AlCo}_x\text{CrFeNi}$ vertical section for $0 < x < 2$.

It can be seen in Fig. 7 that the addition of Co to the equimolar composition destabilizes the A2 phase and slightly increases the

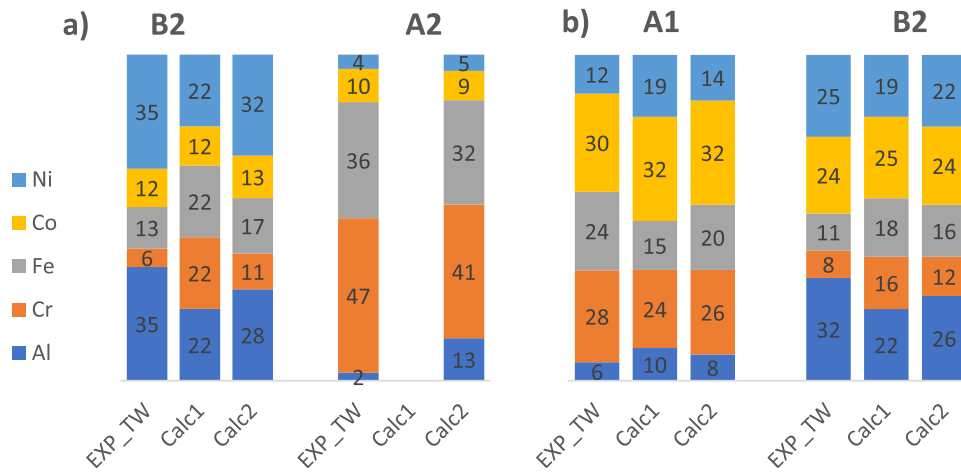


Fig. 8. Experimental phase compositions obtained in this work for samples a) $ACo_{0.5}$ and b) $ACo_{1.5}$ annealed at $1050^{\circ}C$ (EXP_TW) compared with the calculated values before (Calc1) and after (Calc2) optimization.

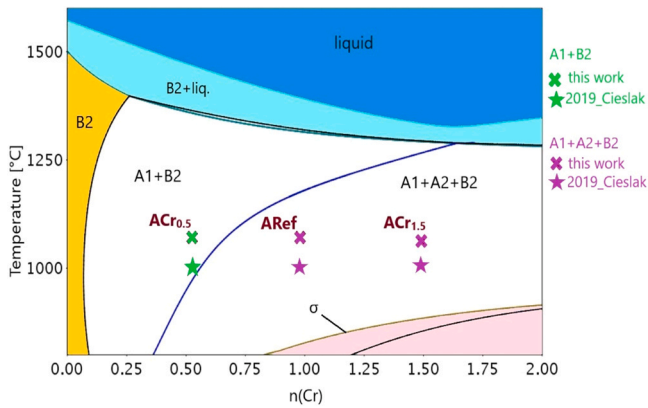


Fig. 9. Calculated vertical section of $AlCoCr_xFeNi$ with the nominal compositions of the samples added. Blue – liquid single phase; yellow – B2 single phase; light blue – liquid present; pink – σ present.

solidus temperature. On the other hand, when the amount of Co is decreased below 0.75 mol, the A1 phase does not form at temperatures above $750^{\circ}C$. The experimentally measured average phase compositions of the samples $ACo_{0.5}$ and $ACo_{1.5}$ are compared in Fig. 8 to the values calculated with the present database before (Calc1) and after (Calc2) the optimization. The improved agreement of Calc2 with experiments can be noticed. Like in the case of the equimolar composition, the calculated amount of Al in the A2 phase is considerably higher than the measured one.

4.2.4. Effect of Cr

The calculated isopleth of $AlCoCr_xFeNi$ ($0 < x < 2$) is shown in Fig. 9 where the nominal compositions of the investigated samples ARef, $ACr_{0.5}$ and $ACr_{1.5}$ are indicated.

It is clear from Fig. 9, that the addition of Cr to the equimolar composition (ARef) increases the stability of A2 and σ phases while a decreasing of the amount of Cr destabilizes the A2 phase which is no longer stable above $750^{\circ}C$ below 0.35 mol of Cr. Another important observation is that the addition of Cr to the quaternary $AlCoFeNi$ alloy significantly decreases the liquidus and solidus temperatures.

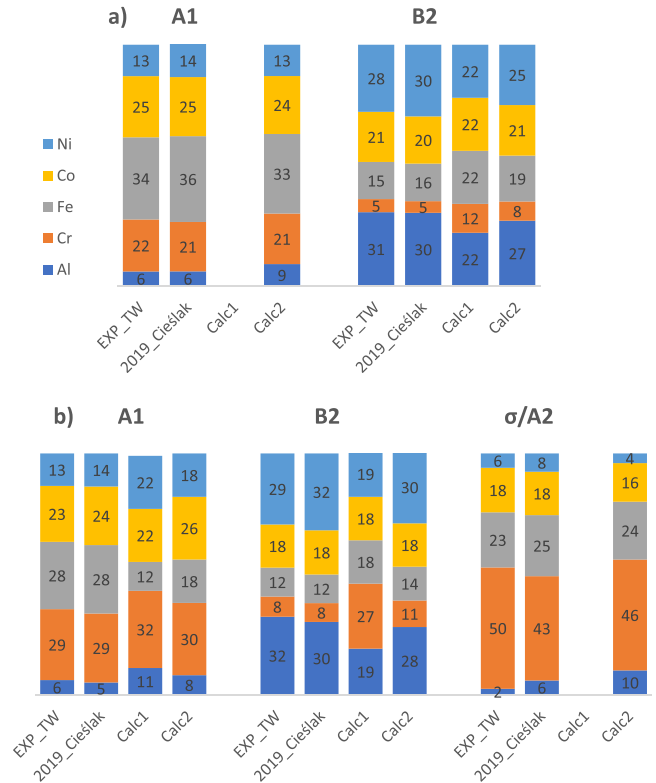


Fig. 10. Experimentally obtained phase compositions in the present work of the samples a) $ACr_{0.5}$ and b) $ACr_{1.5}$ annealed at $1050^{\circ}C$ (EXP_TW) compared with the calculated values before (Calc1) and after (Calc2) optimization and the measured values by Cieslak et al. [54].

The average phase compositions of the samples $ACr_{0.5}$ and $ACr_{1.5}$ measured in the present work are compared in Fig. 10 to the values calculated with the present database before (Calc1) and after (Calc2) optimization, along with the data reported by Cieslak et al. [54]. As mentioned before, we assumed that the σ phase experimentally observed in the $ACr_{1.5}$ sample has formed from the A2 phase during cooling in the air. Therefore, in Fig. 10 the experimentally

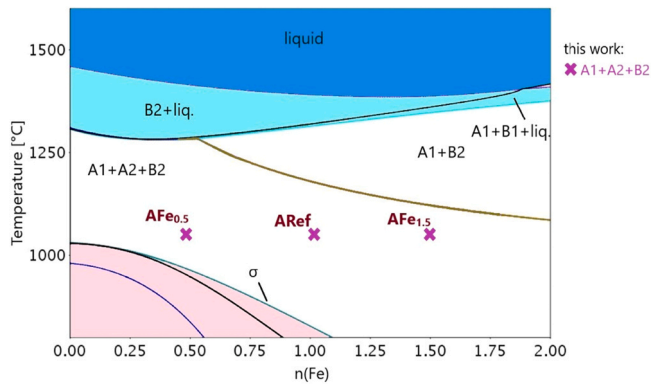


Fig. 11. Calculated vertical section of AlCoCrFe_xNi (0 < x < 2) with the nominal compositions of the samples. Blue – liquid single phase; yellow – B2 single phase; light blue – liquid present; pink – σ present.

determined composition of the σ phase was compared with the calculated composition of the A2 phase. A general good agreement can be observed: only the amount of Fe in A1 phase tends to be lower than the experimental data while its amount in B2 is higher than measured, as it can be seen in Fig. 10b. However, the optimization (Calc2) allowed to minimize the difference.

4.2.5. Effect of Fe

The effect of Fe is shown in Fig. 11, where the isopleth of AlCoCrFe_xNi (0 < x < 2) is calculated with the present database. The nominal compositions of the samples ARef, AFe_{0.5} and AFe_{1.5} are marked in the figure.

As it can be seen in Fig. 11, the addition of Fe destabilizes the A2 phase. Moreover, with the increasing amount of Fe the solidus temperature increases. On the other hand, by removing Fe from the equimolar composition, the σ phase increases its stability and forms at around 1050 °C in the Fe-free alloy.

The measured phase compositions of the AFe0.5 and AFe1.5 samples are compared in Fig. 12 with the values calculated with the present database before (Calc1) and after (Calc2) optimization. Like in the ACr1.5 sample, the σ phase experimentally observed in the AFe0.5 sample was probably formed from the A2 phase during slow cooling. Therefore, in Fig. 12, the experimentally determined composition of the σ phase was compared with the calculated composition of the A2 phase. It can be seen that, similarly to Fig. 10b, an overall good agreement has been obtained. The amount of Fe in the A1 phase tends to be slightly lower than measured, while its value in B2 phase is higher. Another discrepancy is the amount of Al in the A2 phase. Considering the high amount of elements involved in this equilibria, such mismatch is acceptable.

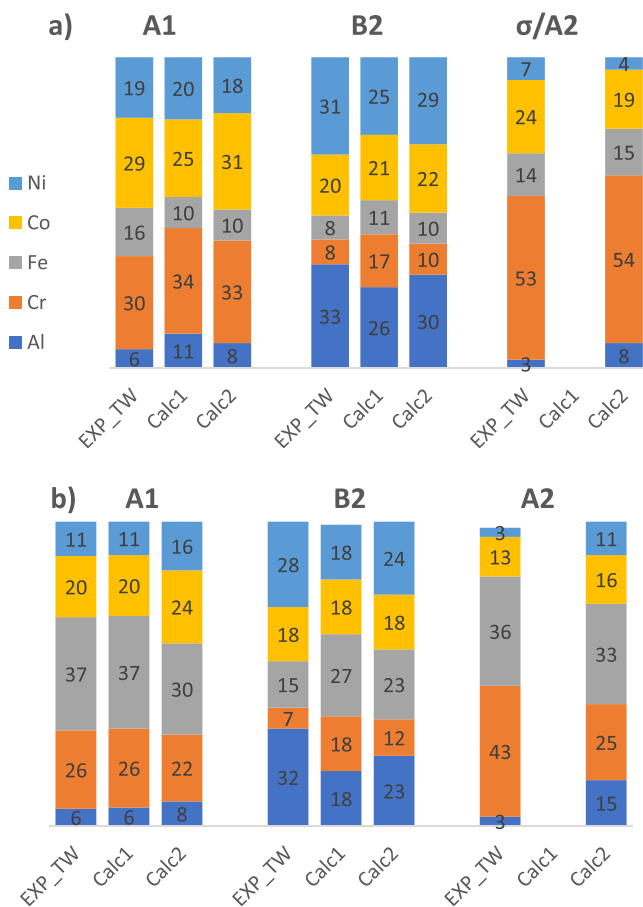


Fig. 12. Experimentally obtained phase compositions in this work of the samples a) AFe_{0.5} and b) AFe_{1.5} annealed at 1050°C (EXP_TW) compared with the calculated values before (Calc1) and after (Calc2) optimization.

4.2.6. Phase amounts

Phase amounts in investigated samples were determined from both XRD profiles and SEM images. Micrographs were analysed with the freeware image processing program ImageJ. Converting the image type to 8-bit and adjusting threshold allowed for the evaluation of the quantity of each phase. Such analysis gave approximate information on phase amounts though with large uncertainty mainly due to the superposition of the gray scale of the different phases used to define the different phase areas. It was especially the case when A2 phase was formed with an intermediate gray shade, as it can be seen in Fig. 2 and Fig. 3. The quantitative analysis of the XRD profiles using Rietveld method allowed for obtaining the quantities of the identified phases, however, even this method has large uncertainty. Most peaks of the disordered and ordered bcc phases overlap with each other, making it difficult to evaluate the quantities of these phases correctly. For all these reasons, the quantities of A2 and B2 phases in Table 5 are merged for comparison with the calculated values.

Considering the uncertainty of the measured values, a good agreement has been obtained between the experiments and the calculations. The largest discrepancy can be observed in case of AFe_{1.5} sample.

Table 5

Phase quantities experimentally obtained from micrographs (SEM) and from XRD profiles (XRD) compared with the calculated values (CALC).

| SAMPLE | ARef | | ACo _{0.5} | | ACr _{0.5} | | ACr _{1.5} | | AFe _{0.5} | | AFe _{1.5} | |
|--------|------|-------|--------------------|------|--------------------|------|--------------------|-------|--------------------|-------|--------------------|-------|
| | A1 | A2+B2 | A1 | B2 | A1 | B2 | A1 | A2+B2 | A1 | A2+B2 | A1 | A2+B2 |
| SEM | 22 | 78 | 52 | 48 | 34 | 66 | 28 | 72 | 16 | 84 | 41 | 59 |
| XRD | 17.8 | 82.2 | 41.4 | 58.6 | 27.1 | 72.9 | 7.9 | 93.1 | 9.4 | 90.6 | 47.9 | 52.1 |
| CALC | 18 | 82 | 45.5 | 54.5 | 20.7 | 79.3 | 12.4 | 87.6 | 13.3 | 86.7 | 23 | 77 |

5. Summary

In the present work the Al-Co-Cr-Fe-Ni system was thermodynamically assessed based on our experimental measurements and data reported in the literature:

- (1) Selected compositions of high entropy alloys from the Al-Co-Cr-Fe-Ni system were prepared by arc-melting and annealed at 1050 °C for 2160 h in order to examine the effects of Co, Cr and Fe on phase stability.
- (2) The samples were analysed by means of SEM, EDS and XRD measurements.
- (3) Three phases were generally observed in the samples: the matrix identified as the B2 ordered phase rich in Al and Ni, the uniformly distributed A1 phase rich in Co, Cr and Fe and, in some cases, a disordered A2/ σ phase rich in Cr precipitated within the A1 phase.
- (4) The phase equilibrium information obtained in the present work and critically selected from the literature were used for the optimization of the Al-Cr-Fe ternary A1 parameters and a metastable quaternary A2 parameter in the Co-Cr-Fe-Ni system.
- (5) The phase compositions measured in the present work and in selected publications from the literature were compared with the calculations, using the multicomponent database developed in the present work. In particular the equimolar alloy at 1000–1150 °C was considered. The measured solidus and liquidus temperatures and the data reported on phase stabilities with varying amount of Al were compared with the calculations and a good agreement was obtained.
- (6) It can be concluded that the thermodynamic database of the Al-Co-Cr-Fe-Ni system developed in the present work has been validated with the available experimental data and can be used for thermodynamic simulations of compositions for which data are not available. Additionally, it can be treated as a basis for calculations of higher order systems when new elements are included.

Declaration of Competing Interest

The authors declare that they have no known competing financial interests or personal relationships that could have appeared to influence the work reported in this paper.

Acknowledgments

B.B and Z.K.L. were supported by a NASA Space Technology Research Fellowship (grant number 80NSSC18K1168). Z.K.L. was also partially supported by the US National Science Foundation under grant CMMI-1825538.

References

- [1] D.B. Miracle, O.N. Senkov, A critical review of high entropy alloys and related concepts, *Acta Mater.* 122 (2017) 448–511, <https://doi.org/10.1016/j.actamat.2016.08.081>
- [2] J. Chen, X. Zhou, W. Wang, B. Liu, Y. Lv, W. Yang, D. Xu, Y. Liu, A review on fundamental of high entropy alloys with promising high-temperature properties, *J. Alloy. Compd.* 760 (2018) 15–30, <https://doi.org/10.1016/j.jallcom.2018.05.067>
- [3] Y.T. Chen, Y.J. Chang, H. Murakami, S. Gorsse, A.C. Yeh, Designing high entropy superalloys for elevated temperature application, *Scr. Mater.* 187 (2020) 177–182, <https://doi.org/10.1016/j.scriptamat.2020.06.002>
- [4] L. Qiao, Aorigele, Z. Lai, J. Zhu, A promising new class of multi-component alloys with exceptional mechanical properties, *J. Alloy. Compd.* 847 (2020), <https://doi.org/10.1016/j.jallcom.2020.155929>
- [5] M. Pole, M. Sadeghilaridjani, J. Shittu, A. Ayyagari, S. Mukherjee, High temperature wear behavior of refractory high entropy alloys based on 4-5-6 elemental palette, *J. Alloy. Compd.* 843 (2020), <https://doi.org/10.1016/j.jallcom.2020.156004>

- [6] M. Wang, Z.L. Ma, Z.Q. Xu, X.W. Cheng, Designing VxNbMoTa refractory high-entropy alloys with improved properties for high-temperature applications, *Scr. Mater.* 191 (2021) 131–136, <https://doi.org/10.1016/j.scriptamat.2020.09.027>
- [7] M. Wang, Y. Lu, T. Wang, C. Zhang, Z. Cao, T. Li, P.K. Liaw, A novel bulk eutectic high-entropy alloy with outstanding as-cast specific yield strengths at elevated temperatures, *Scr. Mater.* 204 (2021) 114132, <https://doi.org/10.1016/j.scriptamat.2021.114132>
- [8] L. Kaufman, H. Bernstein, *Computer calculation of phase diagrams, With Special Reference to Refractory Metals*, Academic Press Inc, New York, 1970.
- [9] M. Hillert, The compound energy formalism, *J. Alloy. Compd.* 320 (2001) 161–176, [https://doi.org/10.1016/S0925-8388\(00\)01481-X](https://doi.org/10.1016/S0925-8388(00)01481-X)
- [10] M. Ostrowska, G. Cacciamani, Critical evaluation and thermodynamic modeling of the Al-Co-Fe system, *J. Alloy. Compd.* 794 (2019) 553–568, <https://doi.org/10.1016/j.jallcom.2019.04.170>
- [11] Z.K. Liu, Computational thermodynamics and its applications, *Acta Mater.* 200 (2020) 745–792, <https://doi.org/10.1016/j.actamat.2020.08.008>
- [12] B. Bocklund, R. Otis, A. Egorov, A. Obaied, I. Roslyakova, Z.-K. Liu, ESPEI for efficient thermodynamic database development, modification, and uncertainty quantification: application to Cu–Mg, *MRS Commun.* 9 (2019) 618–627, <https://doi.org/10.1557/mrc.2019.59>
- [13] R. Otis, Z.-K. Liu, Pycalphad: CALPHAD-based computational thermodynamics in Python, *J. Open Res. Softw.* 5 (2017) 1–11, <https://doi.org/10.5334/jors.140>
- [14] Y. Wang, G. Cacciamani, Experimental investigation and thermodynamic assessment of the Al-Co-Ni system, *Calphad Comput. Coupling Phase Diagr. Thermochem* 61 (2018) 198–210, <https://doi.org/10.1016/j.calphad.2018.03.008>
- [15] F. Stein, C. He, N. Dupin, Melting behaviour and homogeneity range of B2 CoAl and updated thermodynamic description of the Al–Co system, *Intermetallics* 39 (2013) 58–68, <https://doi.org/10.1016/j.intermet.2013.03.011>
- [16] P. Priputen, M. Kusý, M. Drienovský, D. Janičkovič, R. Čička, I. Černíčková, J. Janovec, Experimental reinvestigation of Al–Co phase diagram in vicinity of Al13Co4 family of phases, *J. Alloy. Compd.* 647 (2015) 486–497, <https://doi.org/10.1016/j.jallcom.2015.05.248>
- [17] P. Wang, M.C. Peters, U.R. Kattner, K. Choudhary, G.B. Olson, Thermodynamic analysis of the topologically close packed σ phase in the Co–Cr system, *Intermetallics* 105 (2019) 13–20, <https://doi.org/10.1016/j.intermet.2018.11.004>
- [18] J. Wang, X.G. Lu, N. Zhu, W. Zheng, Thermodynamic and diffusion kinetic studies of the Fe–Co system, *Calphad Comput. Coupling Phase Diagr. Thermochem* 58 (2017) 82–100, <https://doi.org/10.1016/j.calphad.2017.06.001>
- [19] I. Ohnuma, H. Enoki, O. Ikeda, R. Kainuma, H. Ohtani, B. Sundman, K. Ishida, Phase equilibria in the Fe–Co binary system, *Acta Mater.* 50 (2002) 379.
- [20] Y. Wang, G. Cacciamani, Thermodynamic modeling of the Al–Cr–Ni system over the entire composition and temperature range, *J. Alloy. Compd.* 688 (2016) 422–435, <https://doi.org/10.1016/j.jallcom.2016.07.130>
- [21] B. Sundman, I. Ohnuma, N. Dupin, U.R. Kattner, S.G. Fries, An assessment of the entire Al–Fe system including D03 ordering, *Acta Mater.* 57 (2009) 2896–2908, <https://doi.org/10.1016/j.actamat.2009.02.046>
- [22] A.F. Guillermet, Assessment of the thermodynamic properties of the Ni–Co system, *Z. Für Met* 78 (1987) 639–647.
- [23] A. Jacob, E. Povoden-Karadeniz, E. Kozeschnik, Revised thermodynamic description of the Fe–Cr system based on an improved sublattice model of the σ phase, *Calphad* 60 (2018) 16–28, <https://doi.org/10.1016/j.calphad.2017.10.002>
- [24] P. Gustafson, A thermodynamic evaluation of the Cr–Ni–W system, *Calphad* 12 (1988) 277–292, [https://doi.org/10.1016/0364-5916\(88\)90008-9](https://doi.org/10.1016/0364-5916(88)90008-9)
- [25] P. Franke, H.J. Seifert, The influence of magnetic and chemical ordering on the phase diagram of Cr–Fe–Ni, *Calphad-Comp. Coupl. Phase Diagr. Thermochem.* 35 (2011) 148–154, <https://doi.org/10.1016/j.calphad.2010.10.006>
- [26] M. Ostrowska, G. Cacciamani, Thermodynamic modelling of the σ and μ phases in several ternary systems containing Co, Cr, Fe, Mo, Re and W, *J. Alloy. Compd.* 845 (2020) 156122, <https://doi.org/10.1016/j.jallcom.2020.156122>
- [27] X.L. Liu, T. Gheno, B.B. Lindahl, G. Lindwall, B. Gleeson, Z.-K. Liu, First-principles calculations, experimental study, and thermodynamic modeling of the Al–Co–Cr system, *PLOS One* 10 (2015) 0121386.
- [28] E.S. Moskvitina, V.N. Kuznetsov, L.S. Guzei, Refinement of the Co–Cr–Al phase diagram, *Vestn. Mosk. Univ., Ser. Khim.* 33 (1992) 373–374.
- [29] K. Ishikawa, M. Ise, I. Ohnuma, R. Kainuma, K. Ishida, Phase equilibria and stability of the bcc aluminide in the Co–Cr–Al system, *Ber. Der Bunsenges. Für Phys. Chem.* 102 (1998) 1206–1210.
- [30] L. Zhu, S. Soto-Medina, R.G. Hennig, M.V. Manuel, Experimental investigation of the Al–Co–Fe phase diagram over the whole composition range, *J. Alloy. Compd.* 815 (2020) 152110, <https://doi.org/10.1016/j.jallcom.2019.152110>
- [31] S. Wang, Z. Li, Z. Qin, S. Wang, X. Lu, C. Li, Thermodynamic modeling of Al–Fe–Cr ternary system, *Miner. Met. Mater. Ser.* (2017), https://doi.org/10.1007/978-3-319-51493-2_42
- [32] L.J. Zhang, J. Wang, Y. Du, R.X. Hu, P. Nash, X.G. Lu, C. Jiang, Thermodynamic properties of the Al–Fe–Ni system acquired via a hybrid approach combining calorimetry, first-principles and Calphad, *Acta Mater.* 57 (2009) 5324–5341, <https://doi.org/10.1016/j.actamat.2009.07.031>
- [33] M.A.X. Dombre, O.S. Campos, N. Valignat, C. Allibert, C. Bernard, J. Driole, Solid state equilibrium in the ternary Fe–Co–Cr system: experimental determination of isothermal sections in the temperature range 800–1300 °C, *J. Less Common Met.* 66 (1979) 1–11.
- [34] G. Cacciamani, G. Roncallo, Y. Wang, E. Vacchieri, A. Costa, Thermodynamic modelling of a six component (C–Co–Cr–Ni–Ta–W) system for the simulation of cobalt based alloys, *J. Alloy. Compd.* 730 (2017) 291–310, <https://doi.org/10.1016/j.jallcom.2017.09.327>

- [35] W. Köster, W.D. Haehl, The real constitution diagram and the obtention of equilibrium in the ternary system iron-cobalt-nickel, *Arch. Eisenhuettenwes.* 40 (1969) 569–574.
- [36] T. Kase, *Sci. Repts. Tohoku Imp. Univ.* 16 (1927) 491–513.
- [37] J. Miettinen, Thermodynamic reassessment of Fe-Cr-Ni system with emphasis on the iron-rich corner, *Calphad Comput. Coupling Phase Diagr. Thermochem.* 23 (1999) 231–248, [https://doi.org/10.1016/S0364-5916\(99\)00027-9](https://doi.org/10.1016/S0364-5916(99)00027-9)
- [38] Y.F. Kao, T.J. Chen, S.K. Chen, J.W. Yeh, Microstructure and mechanical property of as-cast, -homogenized, and -deformed Al_xCoCrFeNi (0 ≤ x ≤ 2) high-entropy alloys, *J. Alloy. Compd.* 488 (2009) 57–64, <https://doi.org/10.1016/j.jallcom.2009.08.090>
- [39] H.P. Chou, Y.S. Chang, S.K. Chen, J.W. Yeh, Microstructure, thermophysical and electrical properties in Al_xCoCrFeNi (0 ≤ x ≤ 2) high-entropy alloys, *Mater. Sci. Eng. B Solid-State Mater. Adv. Technol.* 163 (2009) 184–189, <https://doi.org/10.1016/j.mseb.2009.05.024>
- [40] R. Wang, K. Zhang, C. Davies, X. Wu, Evolution of microstructure, mechanical and corrosion properties of AlCoCrFeNi high-entropy alloy prepared by direct laser fabrication, *J. Alloy. Compd.* 694 (2017) 971–981, <https://doi.org/10.1016/j.jallcom.2016.10.138>
- [41] O. Stryzhyboroda, V.T. Witusiewicz, S. Gein, D. Röhrsens, U. Hecht, Phase equilibria in the Al-Co-Cr-Fe-Ni high entropy alloy system: thermodynamic description and experimental study, *Front. Mater.* 7 (2020) 1–13, <https://doi.org/10.3389/fmats.2020.00270>
- [42] W.R. Wang, W.L. Wang, S.C. Wang, Y.C. Tsai, C.H. Lai, J.W. Yeh, Effects of Al addition on the microstructure and mechanical property of Al_xCoCrFeNi high-entropy alloys, *Intermetallics* 26 (2012) 44–51, <https://doi.org/10.1016/j.intermet.2012.03.005>
- [43] W.L.W.W.R. Wang, W.L.W.W.R. Wang, J.W. Yeh, Phases, microstructure and mechanical properties of Al_xCoCrFeNi high-entropy alloys at elevated temperatures, *J. Alloy. Compd.* 589 (2014) 143–152, <https://doi.org/10.1016/j.jallcom.2013.11.084>
- [44] T. Yang, S. Xia, S. Liu, C. Wang, S. Liu, Y. Zhang, J. Xue, S. Yan, Y. Wang, Effects of Al addition on microstructure and mechanical properties of Al_xCoCrFeNi High-entropy alloy, *Mater. Sci. Eng. A.* 648 (2015) 15–22, <https://doi.org/10.1016/j.msea.2015.09.034>
- [45] C. Zhang, F. Zhang, H. Diao, M.C. Gao, Understanding phase stability of Al-Co-Cr-Fe-Ni high entropy alloys, *Mater. Des.* 109 (2016) 425–433.
- [46] J.C. Rao, H.Y. Diao, V. Ocelík, D. Vainchtein, C. Zhang, C. Kuo, Z. Tang, W. Guo, J.D. Poplawsky, Y. Zhou, P.K. Liaw, J.T.M. De Hosson, Secondary phases in Al_xCoCrFeNi high-entropy alloys: an in-situ TEM heating study and thermodynamic appraisal, *Acta Mater.* 131 (2017) 206–220, <https://doi.org/10.1016/j.actamat.2017.03.066>
- [47] T. Butler, M. Weaver, Investigation of the phase stabilities in AlNiCoCrFe high entropy alloys, *J. Alloy. Compd.* 691 (2017) 119–129.
- [48] Z. Tang, O.N. Senkov, C.M. Parish, C. Zhang, F. Zhang, L.J. Santodonato, G. Wang, G. Zhao, F. Yang, P.K. Liaw, Tensile ductility of an AlCoCrFeNi multi-phase high-entropy alloy through hot isostatic pressing (HIP) and homogenization, *Mater. Sci. Eng. A* 647 (2015) 229–240, <https://doi.org/10.1016/j.msea.2015.08.078>
- [49] T.T. Shun, Y.C. Du, Microstructure and tensile behaviors of FCC Al_{0.3}CoCrFeNi high entropy alloy, *J. Alloy. Compd.* 479 (2009) 157–160, <https://doi.org/10.1016/j.jallcom.2008.12.088>
- [50] No Title, (n.d.). (<https://www.crystalimpact.com/match/download.htm>).
- [51] J. Rodriguez-Carvajal, Fullprof Program, (1993) 192.
- [52] ThermoCalc Ni-based Superalloys Database, TCNI8, (2015).
- [53] Y. Sun, C. Wu, H. Peng, Y. Liu, J. Wang, X. Su, Phase constituent and microhardness of As-cast and long-time annealed Al_xCo_{2-x}CrFeNi multicomponent alloys, *J. Phase Equilibria Diffus.* 40 (2019) 706–714, <https://doi.org/10.1007/s11669-019-00761-9>
- [54] J. Cieslak, J. Tobola, J. Przewoznik, K. Berent, U. Dahlborg, J. Cornide, S. Mehraban, N. Lavery, M. Calvo-Dahlborg, Multi-phase nature of sintered vs. arc-melted Cr_xAlFeCoNi high entropy alloys - experimental and theoretical study, *J. Alloy. Compd.* 801 (2019) 511–519, <https://doi.org/10.1016/j.jallcom.2019.06.121>